Physics Letters B 804 (2020) 135380

Contents lists available at ScienceDirect

Physics Letters B

www.elsevier.com/locate/physletb

Study of the process $e^+e^- \to K^0_S K^0_S \pi^+\pi^-$ in the c.m. energy range 1.6–2.0 GeV with the CMD-3 detector

R.R. Akhmetshin [a,b], A.N. Amirkhanov [a,b], A.V. Anisenkov [a,b], V.M. Aulchenko [a,b], V.Sh. Banzarov [a], N.S. Bashtovoy [a], D.E. Berkaev [a,b], A.E. Bondar [a,b], A.V. Bragin [a], S.I. Eidelman [a,b,e], D.A. Epifanov [a,b], L.B. Epshteyn [a,b,c], A.L. Erofeev [a,b], G.V. Fedotovich [a,b], S.E. Gayazov [a,b], F.J. Grancagnolo [f], A.A. Grebenuk [a,b], S.S. Gribanov [a,b], D.N. Grigoriev [a,b,c], F.V. Ignatov [a,b], V.L. Ivanov [a,b], S.V. Karpov [a], A.S. Kasaev [a], V.F. Kazanin [a,b], I.A. Koop [a,b], A.A. Korobov [a,b], A.N. Kozyrev [a,c], E.A. Kozyrev [a,b], P.P. Krokovny [a,b], A.E. Kuzmenko [a,b], A.S. Kuzmin [a,b], I.B. Logashenko [a,b], P.A. Lukin [a,b], A.P. Lysenko [a], K.Yu. Mikhailov [a,b], V.S. Okhapkin [a], E.A. Perevedentsev [a,b], Yu.N. Pestov [a], A.S. Popov [a,b], G.P. Razuvaev [a,b], A.A. Ruban [a], N.M. Ryskulov [a], A.E. Ryzhenenkov [a,b], A.V. Semenov [a,b], Yu.M. Shatunov [a], V.E. Shebalin [a,b], D.N. Shemyakin [a,b], B.A. Shwartz [a,b], D.B. Shwartz [a,b], A.L. Sibidanov [a,d], E.P. Solodov [a,b,*], M.V. Timoshenko [a], V.M. Titov [a], A.A. Talyshev [a,b], A.I. Vorobiov [a], I.M. Zemlyansky [a], Yu.V. Yudin [a,b]

[a] *Budker Institute of Nuclear Physics, SB RAS, Novosibirsk, 630090, Russia*
[b] *Novosibirsk State University, Novosibirsk, 630090, Russia*
[c] *Novosibirsk State Technical University, Novosibirsk, 630092, Russia*
[d] *University of Victoria, Victoria, BC, V8W 3P6, Canada*
[e] *Lebedev Physical Institute RAS, Moscow, 119333, Russia*
[f] *Instituto Nazionale di Fisica Nucleare, Sezione di Lecce, Lecce, Italy*

ARTICLE INFO

Article history:
Received 12 December 2019
Received in revised form 3 March 2020
Accepted 17 March 2020
Available online 25 March 2020
Editor: L. Rolandi

ABSTRACT

The cross section of the process $e^+e^- \to K^0_S K^0_S \pi^+\pi^-$ has been measured using a data sample of 56.7 pb^{-1} collected with the CMD-3 detector at the VEPP-2000 e^+e^- collider. 596±27 and 210±18 signal events have been selected with six and five detected tracks, respectively, in the center-of-mass energy range 1.6–2.0 GeV. The total systematic uncertainty of the cross section is about 10%. The study of the production dynamics confirms the dominance of the $K^*(892)^+K^*(892)^-$ intermediate state.

1. Introduction

e^+e^- annihilation into hadrons below 2 GeV is rich for various multiparticle final states. Their detailed studies are important for development of phenomenological models describing strong interactions at low energies. One of the final states, $K^0_S K^0_S \pi^+\pi^-$, has been studied before by the BaBar collaboration [1], based on the Initial-State Radiation (ISR) method. Their analysis showed that below the center-of-mass energy ($E_{\rm c.m.}$) of 2 GeV the process is dominated by the $K^*(892)^+K^*(892)^-$ intermediate state with a small contribution of the $K^0_S K^0_S \rho(770)$ reaction. As a part of the total hadronic cross section, the cross section of $e^+e^- \to K^0_S K^0_S \pi^+\pi^-$ is interesting for the calculations of the hadronic vacuum polarization and, as a consequence, for the hadronic contribution to the muon anomalous magnetic moment [2–4]. Until recently, of various possible charge combinations of the $K\bar{K}\pi\pi$ final state only two were measured ($K^+K^-\pi^+\pi^-$ and $K^+K^-\pi^0\pi^0$). Contributions from other $K\bar{K}\pi\pi$ final states ($K^\pm K^0_S \pi^\mp \pi^0$, $K^0_S K^0_S \pi^0\pi^0$ etc.) were taken into account using isospin relations that resulted in large uncertainties. The measurements of other exclusive reactions, see [5] and references therein, helped decreasing such uncertainties and changed the contribution of such final states to the muon anomalous magnetic moment from 3.31 ± 0.58 to 2.41 ± 0.11 in units of 10^{-10} for the energy range below 2 GeV. The difference

* Corresponding author at: Budker Institute of Nuclear Physics, SB RAS, Novosibirsk, 630090, Russia.
E-mail address: solodov@inp.nsk.su (E.P. Solodov).

https://doi.org/10.1016/j.physletb.2020.135380

Table 1
Energy interval, integrated luminosity, number of signal 6-track events, number of signal 5-track events, detection efficiency, and the obtained cross section for the $e^+e^- \to K^0_S K^0_S \pi^+\pi^-$ reaction. Only statistical uncertainties are shown.

$E_{c.m.}$, MeV	L, nb^{-1}	$N_{6\pi}$	$N_{5\pi}$	ϵ	$\sigma_{K^0_S K^0_S \pi^+\pi^-}$, nb
2007.0±0.5	4259	45 ± 7	19.0 ± 5.0	0.048	0.341 ± 0.047
1980±1	2368	29 ± 6	13.5 ± 4.1	0.053	0.366 ± 0.063
1940–1962	5230	95 ± 10	33.8 ± 6.7	0.055	0.484 ± 0.047
1890–1925	5497	72 ± 9	25.8 ± 5.9	0.059	0.329 ± 0.037
1870–1884	16803	218 ± 17	61.5 ± 10.1	0.061	0.298 ± 0.021
1800–1860	8287	79 ± 11	37.2 ± 7.0	0.064	0.238 ± 0.026
1700–1780	8728	47 ± 8	11.5 ± 4.8	0.066	0.111 ± 0.018
1600–1680	7299	11 ± 4	7.8 ± 3.7	0.068	0.041 ± 0.011

is rather large and the detailed study of the production dynamics can further improve the accuracy of these calculations and understanding of the energy dependence of the cross section.

In this paper we report the analysis of the data sample of 56.7 pb^{-1} collected at the CMD-3 detector in the 1.6–2.0 GeV $E_{c.m.}$ range. These data were collected during four energy scans, with a 5–10 MeV c.m. energy step each, performed at the VEPP-2000 e^+e^- collider [6–9] in the 2011, 2012 and 2017 experimental runs. In 2017 (about half of integrated luminosity) the beam energy was monitored by the back-scattering laser-light system [10,11], providing an absolute beam-energy monitoring with better than 0.1 MeV uncertainty at every 10-20 minutes of data taking. In earlier runs the beam energy was determined using measurements of charged track momenta in the detector magnetic field with an about 1 MeV uncertainty. Since the cross section of the process is small, we combine our scanned points into eight energy intervals as shown in Table 1.

The general-purpose detector CMD-3 has been described in detail elsewhere [12]. Its tracking system consists of a cylindrical drift chamber (DC) [13] and double-layer multiwire proportional Z-chamber, both also used for a charged track trigger, and both inside a thin (0.2 X_0) superconducting solenoid with a field of 1.3 T. The tracking system provides the 98-99% tracking efficiency in about 70% of the solid angle. The liquid xenon (LXe) barrel calorimeter with a 5.4 X_0 thickness has fine electrode structure, providing 1–2 mm spatial resolution for photons independently of their energy [14], and is located in the cryostat vacuum volume outside the solenoid. The barrel CsI crystal calorimeter with a thickness of 8.1 X_0 surrounds the LXe calorimeter, while the endcap BGO calorimeter with a thickness of 13.4 X_0 is placed inside the solenoid [15]. Altogether, the calorimeters cover 0.9 of the solid angle and amplitude signals provide information for the neutral trigger. Charged trigger requires presence of only one charged track in DC, therefore it has practically 100% efficiency for our studied process with five or six detected tracks. A relatively large fraction of these events has sufficient energy deposition in the calorimeter for the independent neutral trigger: these events are used to control the charged trigger efficiency. The luminosity is measured using the Bhabha scattering events at large angles with about 1% systematic uncertainty [16].

To understand the detector response to processes under study and to obtain the detection efficiency, we have developed Monte Carlo (MC) simulation of our detector based on the GEANT4 [17] package, in which all simulated events pass the whole reconstruction and selection procedure. The MC simulation uses primary generators with the matrix elements for the $K^0_S K^0_S \pi^+\pi^-$ final state with the $K^*(892)^+ K^*(892)^-$, $K_1(1400) K^0_S \to K^*(892)^\pm \pi^\mp K^0_S$, and $K_1(1270) K^0_S \to K^0_S \rho(770) K^0_S$ intermediate states. The primary generator with the $K^0_S K^0_S \pi^+\pi^-$ in the phase-space model (PS) has been also developed. The primary generator includes radiation of photons by an initial electron or positron, calculated according to Ref. [20].

2. Selection of $e^+e^- \to K^0_S K^0_S \pi^+\pi^-$ events

The analysis procedure is similar to our study of the production of six charged pions described in Ref. [19]. Candidate events are required to have five or six charged-particle tracks, each having:

- more than five hits in the DC;
- a transverse momentum larger than 40 MeV/c;
- a minimum distance from a track to the beam axis in the transverse plane of less than 6 cm, that allows reconstruction of a decay point of K^0_S at large distances;
- a minimum distance from a track to the center of the interaction region along the beam axis Z of less than 15 cm.

Reconstructed momenta and angles of the tracks for the five- and six-track events are used for further selection.

In our reconstruction procedure we create the list of the $K^0_S \to \pi^+\pi^-$ candidates which includes every pair of oppositely charged tracks, assuming them to be pions, with the invariant mass within ±80 MeV/c^2 from the K^0_S mass [22] and a common vertex point within a spacial uncertainty of the DC. We calculate momentum and energy for each K^0_S candidate taking the value of the K^0_S mass from Ref. [22].

At the first stage of signal event selection we require at least two K^0_S candidates with four independent tracks plus one or two additional charged tracks originating from the collision point. If there are still more than two K^0_S candidates, two candidate pairs with minimal deviations from the K^0_S mass are retained. Additionally, we require the distance from the beam axis for the tracks not from K^0_S to be less than 0.35 cm.

Fig. 1 shows the scatter plot for the invariant mass of the first $K^0_S \to \pi^+\pi^-$ candidate vs the second one for data (a) and MC simulation (b). All energy intervals are combined for the presented histograms in data. The lines show selections for the signal events in the central square and for the background level estimate from the events in other eight squares.

Fig. 2(a) shows the scatter plot for the invariant mass of the $K^0_S \to \pi^+\pi^-$ candidates vs the radial distance of the reconstructed vertex from the beam axis. Events associated with K^0_S are clearly seen as well as the background events. Red dots (in the color version) are for simulation. Fig. 2(b) shows a radial distance from the beam axis for the tracks not associated with the K^0_S decay. The additional requirement for this distance to be less than 0.35 cm is shown by the line.

The central vertical and horizontal bands in Fig. 1 correspond to the events with one wrongly reconstructed K^0_S, which are seen in Fig. 1(b) also for simulation due to a combinatorial effect, or if one of the K^0_S decays to other modes. For data these events can be also due to a possible background, like $e^+e^- \to K^0_S K^\pm \pi^\mp \pi^+\pi^-$ with a misidentified or missing charged kaon, when only one K^0_S is present in the final state: these events contribute to the selected data sample in Fig. 1(a).

While we do not use special ordering for the calculation of the first and second $m(K^0_S)$, the background contribution to the vertical and horizontal bands can be different, and we use the "nine tile" method to extract the number of signal events and estimate the background contribution. In this procedure the two-dimensional plot is divided into nine tiles with equal area as shown in Fig. 1 by lines. The tiles in Fig. 1 are numbered from left to right from top to bottom. The central (signal) tile contains N_5 events with two well-reconstructed K^0_S candidates, while the vertical and horizontal tiles, connected to the central signal tile, are used for an estimate of the background contribution to N_5 from the wrongly reconstructed and single K^0_S events. The four corner tiles are used

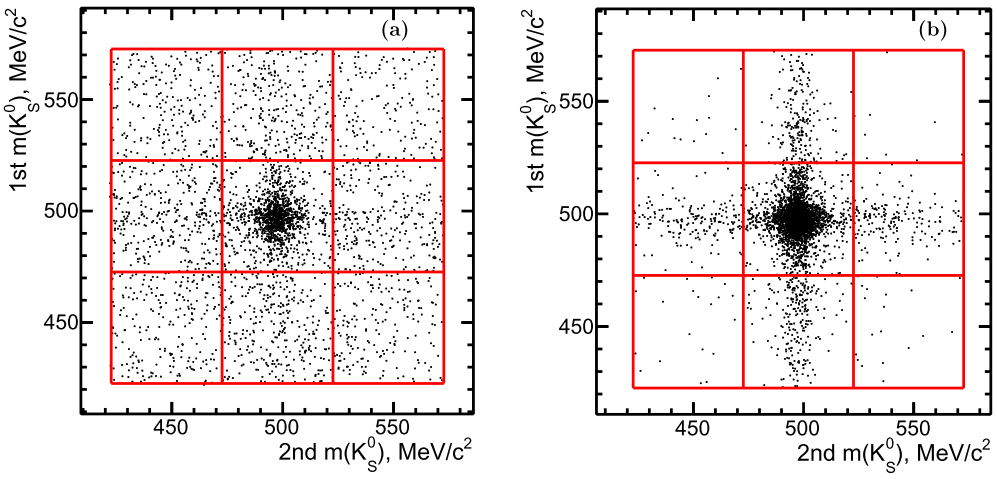

Fig. 1. Scatter plot of the invariant mass of one K^0_S candidate vs invariant mass for the second K^0_S candidate for data (a) and MC simulation (b). The lines show selections for the signal events and for the background level estimate.

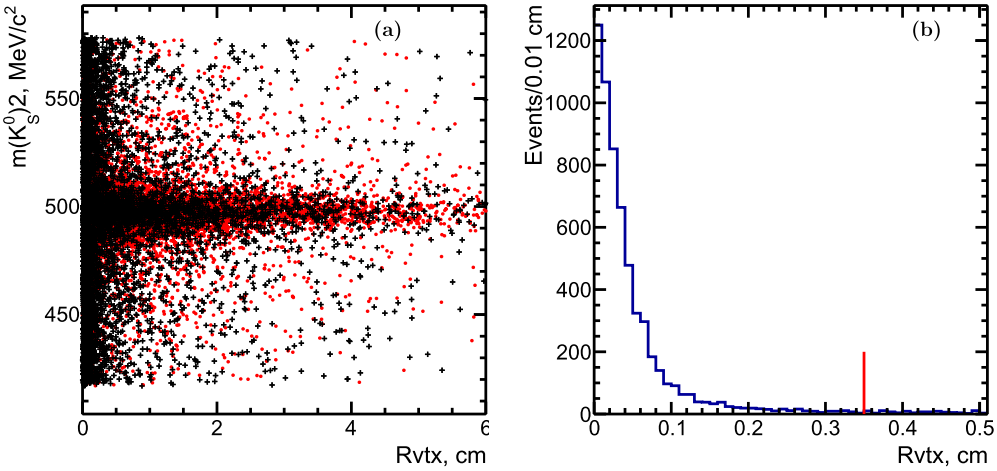

Fig. 2. (a) Scatter plot of the invariant mass of the K^0_S candidate vs the radial distance of the decay vertex (crosses): MC simulation is shown by (red in color version) dots. (b) Radial distance of the not-from-kaon pions from the beam axis. The line shows applied selection.

to estimate the random background. The number of background events in the central tile, $N_{\rm bkg}$, is thus determined as

$$N_{\rm bkg} = (N_2 + N_4 + N_6 + N_8)/2 - (N_1 + N_3 + N_7 + N_9)/4. \quad (1)$$

Note that the random background for a single tile is taken twice from the vertical and horizontal tiles, so the average random background, estimated from the corner tiles, is used for compensation.

At the next stage of event selection, we calculate the expected distribution of any kinematic quantity by weighting the contribution of the eight tiles as in Eq. (1). This is compared to the distribution observed in the signal region.

Fig. 3 shows the histograms for the radial distance of the decay vertex for the $K^0_S \to \pi^+\pi^-$ candidates in the signal region of Fig. 1 for data (a) and simulation at 1900 MeV (b). Points with errors represent the contribution of the background, estimated by the "nine tile" method of Eq. (1). The background from the beam-originating events in data is seen in a few first bins and is well estimated by the method: it is not dominating, so we do not impose any restrictions on this distance. The procedure is also applied to the simulation, and Eq. (1) gives about 5% of the "background" events (Fig. 3(b)) due to only one correctly reconstructed K^0_S or due to small non-linearity of events in the bands, which is assumed to be linear for the method. In our analysis these events are treated in the same way as for data. The systematic uncertainties of the method are discussed below.

For the six- or five-track $K^0_S K^0_S \pi^+\pi^-$ candidates we calculate the total energy of two K^0_S's and two pions: for the five-track candidates the missing momentum is used to calculate the energy of the lost pion. Fig. 4(a) shows the scatter plot of the difference between the total energy and c.m. energy, $E_{\rm tot} - E_{\rm c.m.}$, vs the total momentum of six- (a) or five-track (b) candidates, $P_{\rm tot}$ for data. Events from the central tile of Fig. 1 are shown. A clear signal of the $e^+e^- \to K^0_S K^0_S \pi^+\pi^-$ reaction is seen in Fig. 4(a) as a cluster of crosses near zero, in agreement with the expectation from the simulation shown by (red in the color version) dots. We require $P_{\rm tot}$ to be less than 180 MeV/c^2, thus reducing the number of events with hard radiative photons.

The expected signal of five-track candidates has the $E_{\rm tot} - E_{\rm c.m.}$ value near zero, and the $P_{\rm tot}$ value is distributed up to 500 MeV/c, as shown by the (red) dots from the signal MC simulation in Fig. 4(b). The (black) crosses show our data: signal events are clearly seen.

Fig. 5 shows the projection plots of Fig. 4, $E_{\rm tot} - E_{\rm c.m.}$, for the six-track (a) with applied selection, and the five-track (b) events: the histograms present events from the signal tile, while dots with errors are our estimate of the background contribution using Eq. (1). All energy intervals are summed.

To obtain the number of signal events, we use distributions of Fig. 5 for the $E_{\rm tot} - E_{\rm c.m.}$ difference, i.e. $N_{\rm sig} = N_5 - N_{\rm bkg}$. We subtract the estimated background for each energy interval for six-

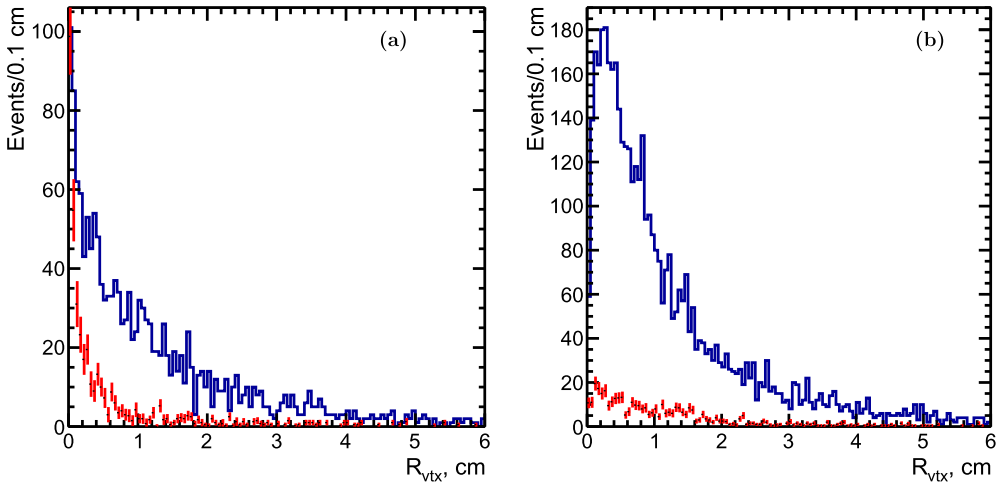

Fig. 3. Radial distance of the decay vertex for the $K^0_S \to \pi^+\pi^-$ candidates in the signal region of Fig. 1 for data (a) and simulation (b). Dots with errors represent the background contribution estimated from Eq. (1).

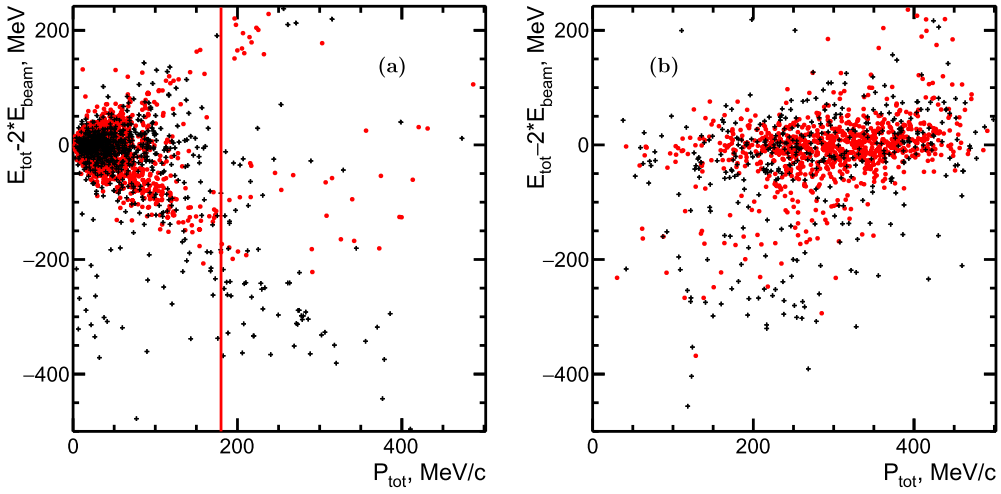

Fig. 4. (a) Scatter plot of the difference between the energy of $K^0_S K^0_S \pi^+\pi^-$ candidates and c.m. energy vs total momentum for events with six tracks. The crosses are for data, while the signal simulation is shown by red (in color version) dots; the line shows the applied selection. (b) Scatter plot of the difference between the energy of $K^0_S K^0_S \pi^+\pi^-$ candidates and c.m. energy vs total momentum for events with five tracks. The crosses are for data, while the signal simulation is shown by red (in color version) dots.

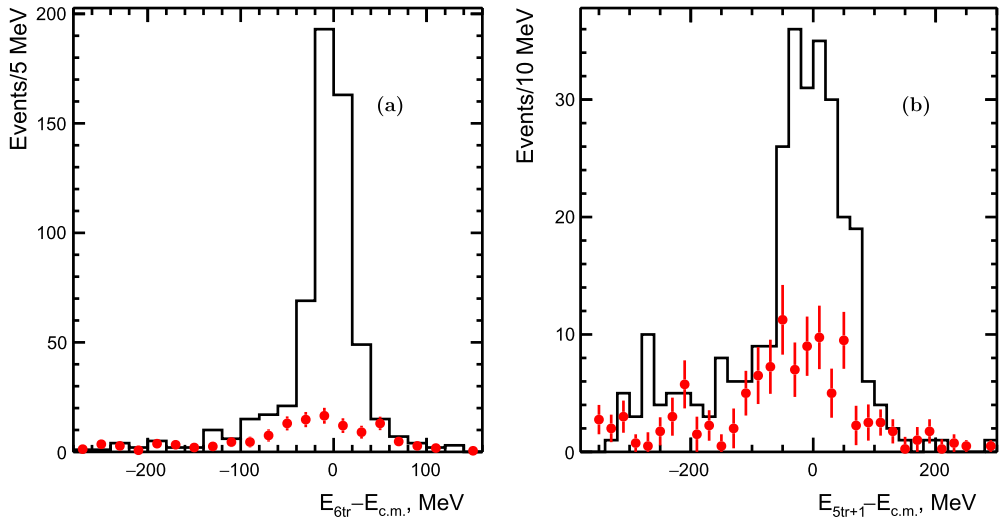

Fig. 5. (a) The difference between the energy of the $K^0_S K^0_S \pi^+\pi^-$ candidates and c.m. energy after selection by the line in Fig. 4 for six-track events (a) and five-track events (b). All the energy intervals are summed. The dots with errors show the background contribution.

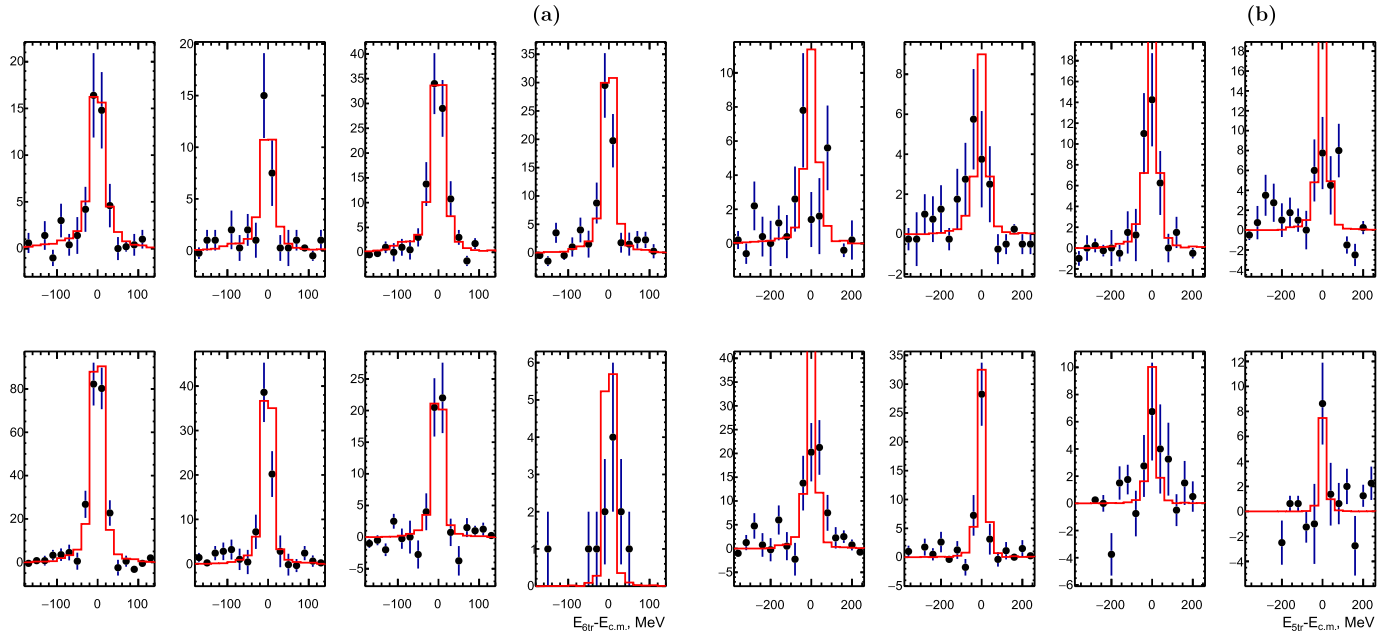

Fig. 6. (a) The difference between the energy of the $K^0_S K^0_S \pi^+\pi^-$ candidates and c.m. energy after background subtraction for six-track (a) and five-track events (b) for eight c.m. energy intervals (dots): left to right, top to bottom according to Table 1. Histograms show expected signals from simulation, normalized to the total number of events in each plot.

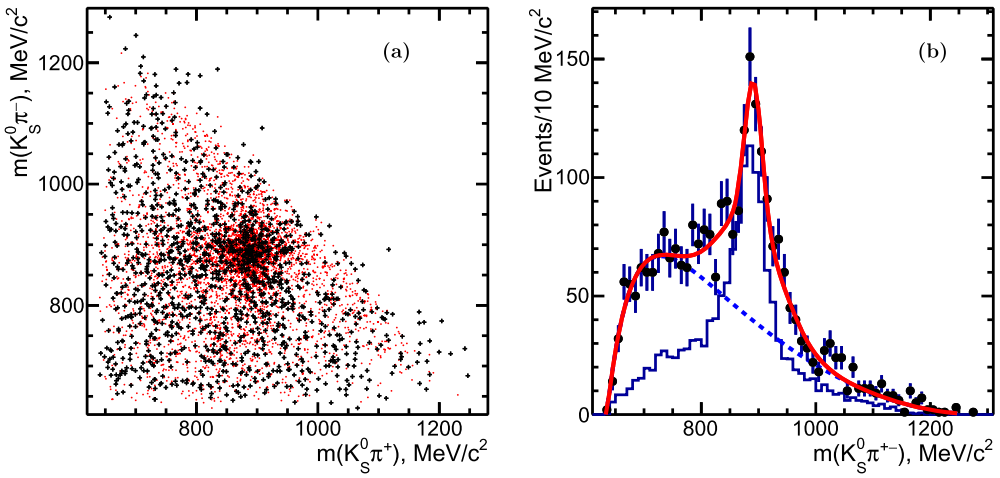

Fig. 7. (a) Experimental $K^0_S\pi^-$ vs $K^0_S\pi^+$ invariant mass distribution (two entries per event, crosses) for the events from the signal region of Fig. 1. Dots (red in color version) show the simulated distribution for the $K^*(892)^+K^*(892)^-$ intermediate state. (b) Projection plot of (a) (four entries per event) with the fit function (solid curve) to determine the number of events with the $K^*(892)$ signal over the background distribution (dotted curve). The histogram shows the corresponding number of simulated events for the $K^*(892)^+K^*(892)^-$ intermediate state.

and five-track events, and count remaining events in the ±100 MeV region for the six-track events, and in the ±200 MeV region for the five-track events. The obtained differences are shown in Fig. 6 by dots for six- (a) and five-track (b) events: from left to right, from top to bottom according to energy intervals of Table 1. The histograms show expected signals from the simulation. In total, we obtain 596±27 and 210±18 for six- and five-track signal events, respectively. The numbers of selected events determined in each energy interval are listed in Table 1.

3. Study of the production dynamics

First attempts to study the dynamics of the process $e^+e^- \to K^0_S K^0_S \pi^+\pi^-$ were carried out by the BaBar Collaboration [1]. They reported the observation of the $e^+e^- \to K^*(892)^+K^*(892)^-$, $K^*(892)^\pm\pi^\mp K^0_S$, $K^0_S K^0_S \rho(770)$ processes, which contribute to the $K^0_S K^0_S \pi^+\pi^-$ final state, with a dominant production of the $K^*(892)^+K^*(892)^-$ intermediate state for the c.m. energies below 2.5 GeV. In the model of the $K\bar{K}\pi^+\pi^-$ production the $K_1(1400)K^0_S$ intermediate state decays to $K^*(892)^\pm\pi^\mp K^0_S$, while $K_1(1270)K^0_S$ can be observed in the $K^0_S K^0_S \rho(770)$ state.

Fig. 7(a) shows the scatter plot of the $K^0_S\pi^-$ invariant mass vs $K^0_S\pi^+$ (two entries/event, all energy intervals are summed) for the $K^0_S K^0_S \pi^+\pi^-$ six-track candidates. A clear signal of the correlated production of the pair of charged $K^*(892)$'s is seen (crosses), in agreement with the expected distribution for the simulated $e^+e^- \to K^*(892)^+K^*(892)^-$ reaction (dots). Fig. 7(b) shows the projection plot of (a) (four entries per event) which we fit with the sum of a double-Gaussian distribution for the $K^*(892)$ signal and a polynomial function for the background. The background includes also wrongly assigned $K^0_S\pi$ combinations. Gaussian parameters are taken from the simulated histogram shown

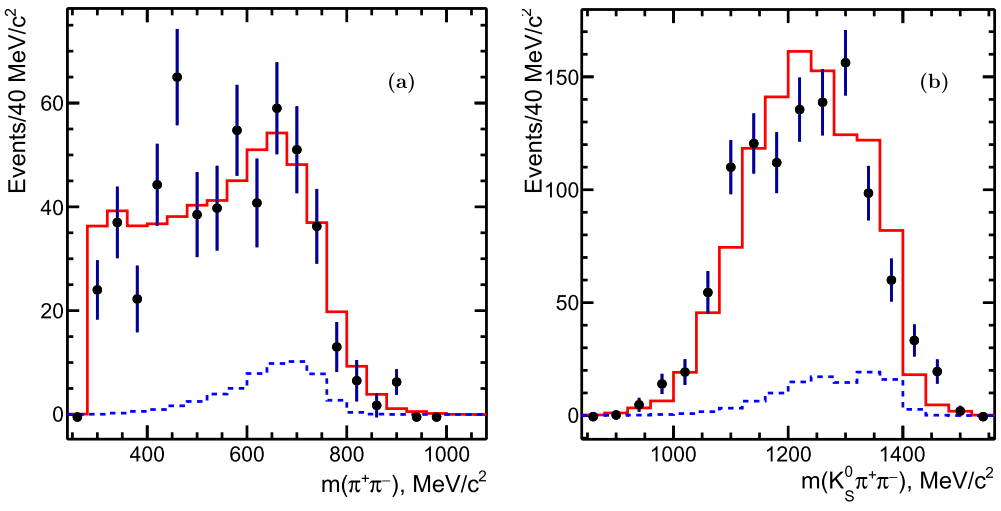

Fig. 8. (a) The background-subtracted $\pi^+\pi^-$ invariant mass distribution (dots) in comparison with the simulated distribution (solid histogram). (b) The background-subtracted $K^0_S\pi^+\pi^-$ (two entries per event) invariant mass distribution (dots) in comparison with the simulated one (a solid histogram). In both plots the simulated distribution includes the $K^*(892)^+K^*(892)^-$ intermediate state plus 30% of the $K_1(1270)K^0_S$, which contribution is shown by a dotted histogram.

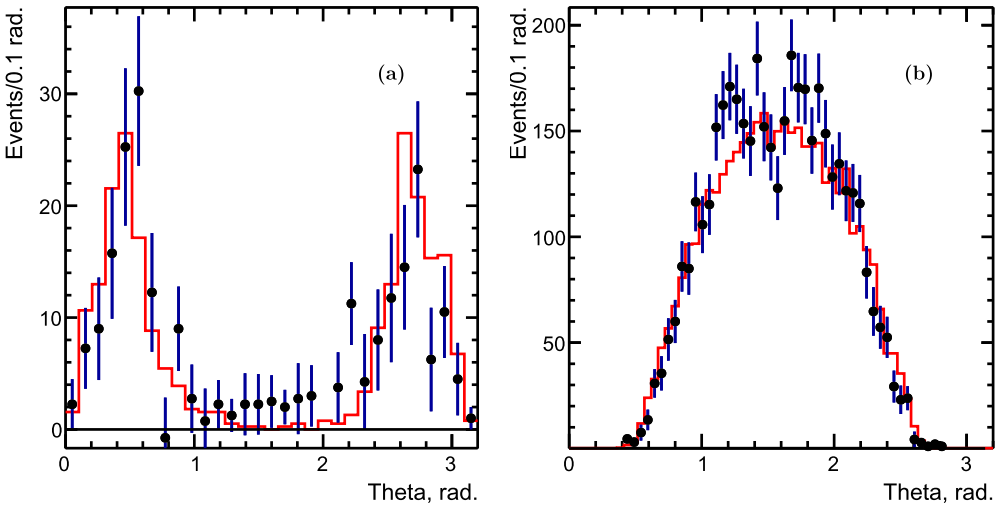

Fig. 9. (a) The background-subtracted experimental (dots) polar angle distribution in comparison with the simulated distribution (histograms) for the missing pion (a) and all detected pions (b).

in Fig. 7(b). The fit yields 788±73±95 events: a second uncertainty is from a variation of the fit functions. Each event from the $K^*(892)^+K^*(892)^-$ reaction contributes twice, so a half of this value should be compared to 596 ± 27, the total number of the six-track signal events. The obtained number indicates that the contribution of the $K^*(892)^+K^*(892)^-$ intermediate state does not exceed $66 \pm 11\%$.

With our data we cannot quantitatively extract a contribution from production of a single $K^*(892)$ or from events without $K^*(892)$'s.

We calculate the background-subtracted invariant mass for the two pions in the six-track sample, not originating from K^0_S, shown in Fig. 8(a), and for the $K^0_S\pi^+\pi^-$ invariant mass (two entries per event), shown in Fig. 8(b). These distributions indicate that the $\rho(770)$ resonance in the $\pi^+\pi^-$ invariant mass, and the $K_1(1270)$ resonance in the $K^0_S\pi^+\pi^-$ invariant mass distribution cannot be excluded. The solid histograms show the simulated distributions of the $K^*(892)^+K^*(892)^-$ intermediate state summed with the 30% contribution from the $K_1(1270)K^0_S \to K^0_SK^0_S\rho(770)$ intermediate state. The latter contribution is shown by the dotted histogram. With the current data sample we cannot quantitatively extract this contribution.

4. Detection efficiency

In our experiment, the acceptance of the DC for charged tracks is not 100%, and the detection efficiency depends on the production dynamics of the reaction as well as on the track reconstruction efficiency in the DC.

To obtain the detection efficiency, we simulate $K^0_SK^0_S\pi^+\pi^-$ production in the primary generators, 50000 events for each c.m. energy interval for each model, pass simulated events through the CMD-3 detector using the GEANT4 [17] package, and reconstruct them with the same software as experimental data. We calculate the detection efficiency from the MC-simulated events as a ratio of events after the selections described in Secs. 2, 3 to the total number of generated events.

Our selection of six- and five-track signal events allows us to estimate a difference in the tracking efficiency in data and simulation. Fig. 9 shows by dots the background-subtracted polar angle for a missing pion (a) and for all detected pions (b). The histogram

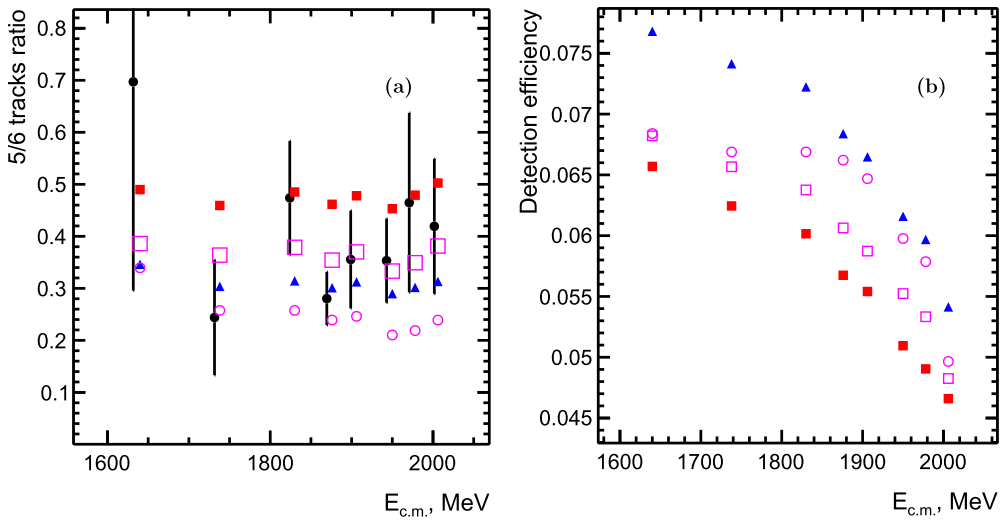

Fig. 10. (a) The ratio of the number of five- to six-track events for data (dots) and simulation for the different intermediate states: phase space model (squares), $K^*(892)^+K^*(892)^-$ intermediate state (open squares), $K_1(1400)K_S^0$ (triangles), and $K_1(1270)K_S^0$ intermediate state (open circles). (b) Detection efficiency obtained from the MC simulation for the $e^+e^- \to K_S^0K_S^0\pi^+\pi^-$ reaction for the different intermediate states (symbols legend is the same as for (a)).

represents the simulated distribution for the $K^*(892)^+K^*(892)^-$ intermediate state. We observe reasonable agreement for data and simulation in these distributions as well as in the calculated ratio of the number of five- to six-track events at each c.m. energy interval, shown in Fig. 10 (a) by open squares. The values of the ratio for the phase-space model (squares), $K_1(1400)K_S^0$ (triangles), and $K_1(1270)K_S^0$ intermediate state (open circles) are also shown in Fig. 10(a) and they are less compatible with data.

We calculate the detection efficiency for the sum of events with six and five detected tracks. Fig. 10(b) shows the detection efficiencies obtained for the $e^+e^- \to K_S^0K_S^0\pi^+\pi^-$ reaction for different intermediate states: markers are the same as for Fig. 10 (a). The detection efficiencies for different modes are relatively close, and the efficiencies calculated for the $K^*(892)^+K^*(892)^-$ intermediate state only and calculated with a 30% contribution from the $K_1(1270)K_S^0$ reaction differ by less or about 5%.

5. Cross section calculation

In each energy interval the cross section is calculated as

$$\sigma = \frac{N_{6\pi} + N_{5\pi}}{L \cdot \epsilon \cdot (1+\delta)},$$

where $N_{6\pi}$, $N_{5\pi}$ are the background-subtracted numbers of signal events with six and five tracks, L is the integrated luminosity for this energy interval, ϵ is the detection efficiency, and $(1+\delta)$ is the radiative correction calculated according to Ref. [20,21]. To calculate the radiative correction, we use BaBar data for the $e^+e^- \to K_S^0K_S^0\pi^+\pi^-$ reaction [1] as a first approximation, and obtain $(1+\delta) = 0.92$ with very weak energy dependence.

We calculate the cross sections for the $e^+e^- \to K_S^0K_S^0\pi^+\pi^-$ reactions using the efficiency shown by open squares in Fig. 10(b) for the $K^*(892)^+K^*(892)^-$ intermediate state. The cross section is shown in Fig. 11. We also calculate the cross section by using only events with six detected tracks: a less than 5% difference is observed.

The energy interval, integrated luminosity, the number of six- and five-track events, efficiency, and the obtained cross section for each energy interval are listed in Table 1.

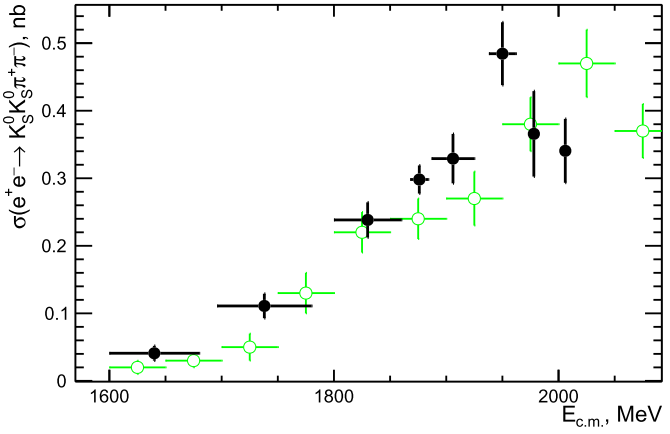

Fig. 11. The $e^+e^- \to K_S^0K_S^0\pi^+\pi^-$ cross section measured with the CMD-3 detector at VEPP-2000 (circles). The results of the BaBar measurement [1] are shown by open circles.

6. Systematic uncertainties

The following sources of systematic uncertainties are considered.

- The tracking efficiency was studied in detail in our previous papers [18,19], and the correction for the track reconstruction efficiency compared to the MC simulation is about 1.0±1.0% per track. Since we add events with one missing track (from the two not from K_S^0), the MC-simulated detection efficiency is corrected by (–5±3)%: the uncertainty is taken as the corresponding systematic uncertainty.
- The model dependence of the acceptance is determined by comparing efficiencies calculated for the different production dynamics. The maximum difference of the detection efficiencies of the dominant $K^*(892)^+K^*(892)^-$ intermediate state and those for other states is about 15%. a possible admixture (of about 30%) of other states changes the efficiency by about 5%, what is taken as the systematic uncertainty estimate.
- Since only one charged track is sufficient for a trigger (98–99% single track efficiency), and using a cross check with the independent neutral trigger, we conclude that for the multitrack

events the trigger inefficiency gives a negligible contribution to the systematic uncertainty.
- The systematic uncertainty due to the selection criteria is studied by varying the requirements described above and doesn't exceed 5%.
- The uncertainty on the determination of the integrated luminosity comes from the selection criteria of Bhabha events, radiative corrections and calibrations of DC and CsI and does not exceed 1% [16].
- The uncertainty in the background subtraction is studied by the variation of the tile dimensions (20×20, 25×25, and 30×30 MeV/c^2 dimensions tested), and by the comparison of the cross section calculated using only six-track events. A less than 5% difference is observed.
- The radiative correction uncertainty is estimated as about 2%, mainly due to the uncertainty on the maximum allowed energy of the emitted photon, as well as from the uncertainty on the cross section.

The above systematic uncertainties summed in quadrature give an overall systematic error of about 10%.

7. Conclusion

The total cross section of the process $e^+e^- \to K^0_S K^0_S \pi^+\pi^-$ has been measured using 56.7 pb^{-1} of integrated luminosity collected by the CMD-3 detector at the VEPP-2000 e^+e^- collider in the 1.6–2.0 GeV c.m. energy range. The systematic uncertainty is about 10%. From our study we can conclude that the observed cross section can be described by the $e^+e^- \to K^*(892)^+K^*(892)^-$ reaction, but an about 30–35% contribution of the $K_1(1270)K^0_S$ intermediate state is not excluded. The measured cross section for the $e^+e^- \to K^0_S K^0_S \pi^+\pi^-$ reaction agrees with the only available measurement by BaBar [1].

Declaration of competing interest

The authors declare that they have no known competing financial interests or personal relationships that could have appeared to influence the work reported in this paper.

Acknowledgements

The authors are grateful to A.I. Milstein for his help with theoretical interpretation and development of the models. We thank the VEPP-2000 team for excellent machine operation. The work is partially supported by the Russian Foundation for Basic Research grant 17-02-00897.

References

[1] J.P. Lees, et al., BaBar Collaboration, Phys. Rev. D 89 (2014) 092002.
[2] M. Davier, A. Hoecker, B. Malaescu, Z. Zhang, Eur. Phys. J. C 77 (2017) 827.
[3] F. Jegerlehner, Acta Phys. Pol. B 49 (2018) 1157.
[4] A. Keshavarzi, D. Nomura, T. Teubner, Phys. Rev. D 97 (2018) 114025.
[5] J.P. Lees, et al., BaBar Collaboration, Phys. Rev. D 95 (2017) 092005.
[6] V.V. Danilov, et al., in: Proceedings EPAC96, Barcelona, 1996, p. 1593.
[7] I.A. Koop, Nucl. Phys. B, Proc. Suppl. 181–182 (2008) 371.
[8] P.Yu. Shatunov, et al., Phys. Part. Nucl. Lett. 13 (2016) 995.
[9] D. Shwartz, et al., PoS ICHEP2016 (2016) 054.
[10] E.V. Abakumova, et al., Phys. Rev. Lett. 110 (2013) 140402.
[11] E.V. Abakumova, et al., J. Instrum. 10 (2015) T09001.
[12] B.I. Khazin, Nucl. Phys. B, Proc. Suppl. 181–182 (2008) 376.
[13] F. Grancagnolo, et al., Nucl. Instrum. Methods 623 (2010) 114.
[14] A.V. Anisyonkov, et al., Nucl. Instrum. Methods 598 (2009) 266.
[15] D. Epifanov, CMD-3 Collaboration, J. Phys. Conf. Ser. 293 (2011) 012009.
[16] R.R. Akhmetshin, et al., Nucl. Phys. B, Proc. Suppl. 225–227 (2012) 69.
[17] S. Agostinelli, et al., GEANT4 Collaboration, Nucl. Instrum. Methods A506 (2003) 250.
[18] R.R. Akhmetshin, et al., CMD-3 Collaboration, Phys. Lett. B 768 (2017) 345.
[19] R.R. Akhmetshin, et al., CMD-3 Collaboration, Phys. Lett. B 723 (2013) 82.
[20] E.A. Kuraev, V.S. Fadin, Sov. J. Nucl. Phys. 41 (1985) 466.
[21] S. Actis, et al., Eur. Phys. J. C 66 (2010) 585.
[22] M. Tanabashi, et al., Particle Data Group, Phys. Rev. D 98 (2018) 030001.